STEM Education

STEM Education, 1 (1): 17–31
DOI: 10.3934/steme.2021002
Received: October 2020
Revised: January 2021

https://www.aimsciences.org/journal/A0000-0006

*Research article*

# Redundancy understanding and theory for robotics teaching: application on a human finger model

**Med Amine Laribi[1,*] and Saïd Zeghloul[1]**

[1] Dept. GMSC, Prime Institute, CNRS - University of Poitiers - ENSMA - UPR 3346, Poitiers, France; said.zeghloul@univ-poitiers.fr (S.Z.)
* **Correspondence:** med.amine.laribi@univ-poitiers.fr; Tel: +5-49-496552

Academic Editor: Giuseppe Carbone

**Abstract:** This paper introduces the concept of redundancy in robotics to students in master degree based on a didactic approach. The definition as well as theoretical description related to redundancy are presented. The example of a human finger is considered to illustrate the redundancy with biomechanical point of view. At the same time, the finger is used to facilitate the comprehension and apply theoretical development to solve direct and inverse kinematics problems. Three different tasks are considered with different degree of redundancy. All developments are implemented under Matlab and validated in simulation on CAD software.

**Keywords:** robotics, redundancy, Matlab, human finger, direct kinematic problem, inverse kinematic problem

## 1. Introduction

A robot is mechanically constructed by connecting a set of links to each other using various types of joints. Actuators provide forces or torques yielding the robot's links to move. Generally, an end-effector is attached to a last specific link [1]. The robot configuration allows to define a whole specification of the position of every point of the robot [2]. The minimum number n of coordinates $q_n$ needed to represent the configuration is the number of degrees of freedom (dof) of the robot. The all possible configurations of the robot are included in a n-dimensional space called the configuration space (C-space). The workspace (W-space) is a description of the configurations that the end-effector

of the robot can reach. The workspace definition is deduced from the robot's structure, independently of the task. The task space (T-space) is a space in which the robot's task can be defined. Both the task space and the workspace are linked to user choice; more general, the orientation is not represented and T-space and W-space are limited to some freedoms of the end-effector.

The task space and the workspace are distinct from the robot's C-space. A point in the task space or the workspace may be reachable by at least one configuration of the robot. If a point in W-space is archived by more than one configuration of the robot, this point is considered with multiples-configurations. This situation is frequently encountered in case of kinematic redundancy [3].

A robot is termed kinematically redundant when it possesses more degrees of freedom than it is needed to execute a given task [4]. Redundancy can be conveniently exploited to achieve more dexterous robot motions [5, 6]; accordingly, the robot presents multiples configurations to access to a specific point in space.

A robot is kinematical redundant for the task if $n > r$ where:

- $n$ the degrees of freedom of the structure (usually the number of the joints).
- $m$ the number of variables needed to describe the task space.
- $r$ the number of variables of the task space needed to describe a task.

In other words, we can say that a robot is redundant when it has more degrees of freedom than strictly needed for describing and executing the task [7]. By the way the redundancy is a relative concept, a robot could be redundant for a task but not for another one [8]. In terms of operational space (T-space or W-space) and configuration space, a manipulator is intrinsically redundant when the dimension of the operational space is smaller than the dimension of the configuration space: $m < n$. A generic task can be represented in the space with 6 variables (3 positional and 3 orientational values). For this reason, a robot that has more than 6 degrees of freedom is intrinsically redundant.

Redundant robots don't add additional complexity to the resolution of the direct kinematics. It is different for the inverse kinematics, where increasing the degrees of freedom the solutions in terms of joints that realize a certain position of the end effector in the space become potentially infinite. For this reason, it is necessary to add additional complexity to kinematic inversion, in order to solve the problem, selecting a solution according to a certain methodology.

The system given by the kinematic model of redundant robot presents a nonempty null-space that allows adequate changes improving robot performances by using the redundant DOFs [9, 10]. This analytical arrangement is feasible due to the pseudoinverse which not affect the null-space. Thus, the solution still affective despite the element modifications of the pseudo-inverse [7]. It is possible to take advantage to this adding some interesting control task like: stay within the feasible joint ranges, avoid kinematic singularities, avoid collision with obstacles, uniformly distribute/limit joint velocities and/or accelerations, increase manipulability in specified directions, optimize execution time and minimize needed motion torques

The human hand presents a captivating object on which researchers in both biomechanics and robotics lead and continue to lead many studies [9, 11]. In this work a human finger with four-joints is modelled as an open chain redundant robot. The finger model is used to introduce the concept of redundancy to students in master degree base on a didactic approach.

This paper focuses on the redundancy definition and its theoretical description through the example of the human finger in didactic way helping the students to more understand the robotic concept. The paper is organised as follows: Section 2 presents the architecture as well as kinematic

model of a finger with biomechanical point of view. Three tasks are defined. Section 3 presents the methods to solve the redundant problem, i.e. geometric method and pseudo-inverse method. Numerical implementation and validation of each method used to solve redundancy to perform the three tasks is presented in section 4. Solutions are illustrated using simulation under CAD model with MECA3D software. Finally, the concluded remarks are summarized in section five.

## 2. Finger kinematics model.

The human hand can be considered as tree structure composed by a base and five serial chains which each one corresponds to a one finger (4 long fingers and a thumb) [12]. Each finger can be considered with 4 actuated degree of freedoms. The kinematic diagram of a single finger is presented in Figure 1.

Let a point P on the fingertip that go through a trajectory $T_i$ during the finger motion. Each joint on the finger is defined by an angle $q_k$ with $k \in \{1,2,3,4\}$ that define the finger configuration.

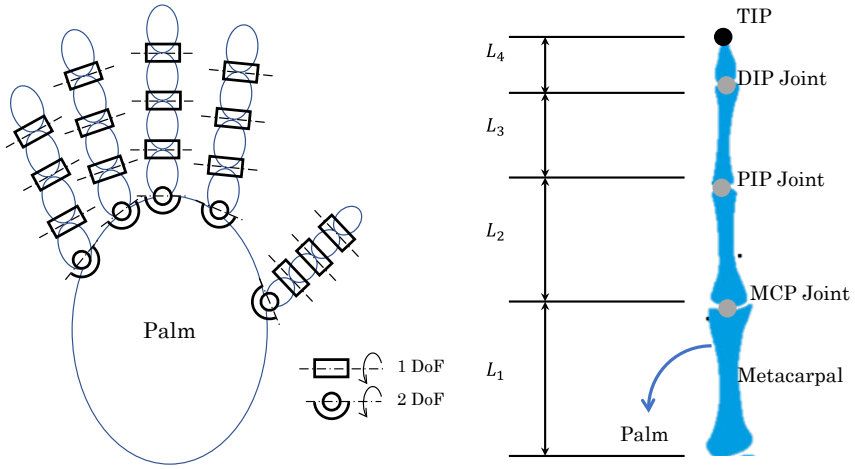


**Figure 1.** Schematic representation of the hand.

In order to analytically identify the direct geometric model (DGM) of a finger as serial robot, the kinematic diagram in the Figure 2 is considered.

Index and Middle fingers are represented as open serial chains with metacarpophalangeal (MCP), proximal interphalangeal (PIP) and distal interphalangeal (DIP) joints. A single dof at the PIP, MCP and DIP joints, and two dof at the palm joint are modelled.

Three tasks described in Table 1 is to be performed by the finger. An initial configuration as well as a displacement of the end-effector, fingertip, are given for each task. The fingertip displacement is performed in the $(x_1, z_1)$ plane and given by the trajectory of point P. Here we consider the angle $q_1$ at the palm joint as unchanged since the finger motion is performed in a plane.

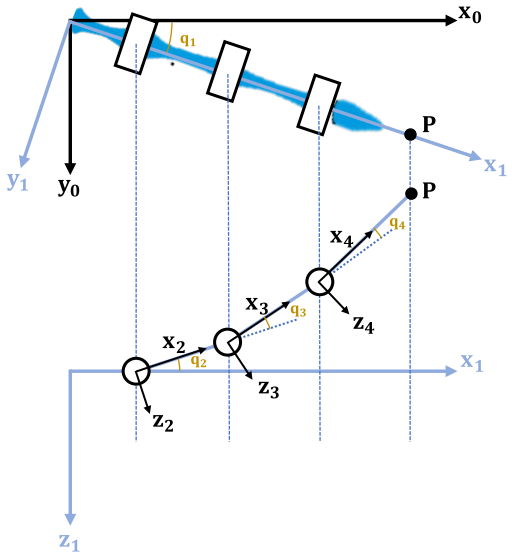


**Figure 2.** Kinematic diagram of a single finger.

**Table 1.** The three tasks of the finger in the $(x_1, z_1)$ plane.

| Task | Initial Configuration | End-effector displacement |
|---|---|---|
| **T1** | $q_2 = 45°,\ q_3 = 90°,\ q_4 = 30°$ | 60 mm along $x_1$ |
| **T2** | $q_2 = 45°,\ q_3 = 45°,\ q_4 = 45°$ | 40 mm along $z_1$ |
| **T3** | $q_2 = 0°,\ q_3 = 45°,\ q_4 = 45°$ | 30 mm along $-x_1$ et 20 mm along $z_1$ |

The degree of redundancy is computed for each task based on $n$ the degrees of freedom and $m$ the number of variables needed to describe the task space as given in Table 2.

**Table 2.** Degree of redundancy

| Task | Degree of redundancy $(n - m)$ |
|---|---|
| **T1** | 2 |
| **T2** | 2 |
| **T3** | 1 |

The direct kinematic model (DKM) of the finger is given by the coordinates of point P in the plane $(x_1, z_1)$ for a configuration given by the joint variables $q_2$, $q_3$ and $q_4$.

$$\mathbf{X}_{\mathrm{P}}^{1} = \mathbf{T}^{14}\mathbf{X}_{\mathrm{P}}^{4} \tag{1}$$

Where, $\mathbf{T}^{14} = \mathbf{T}^{12}\,\mathbf{T}^{23}\,\mathbf{T}^{34}$ the homogeneous matrix defined according to the kinematic diagram in Figure.

The DGM is obtained after arrangement of equation (2) as

$$\begin{cases} x_1 = l_4\cos(q_2+q_3+q_4) + l_3\cos(q_2+q_3) + l_2\cos q_2 + l_1 \\ y_1 = 0 \\ z_1 = -l_4\sin(q_2+q_3+q_4) - l_3\sin(q_2+q_3) - l_2\sin q_2 \end{cases} \tag{2}$$

The direct kinematic model (DKM) can be computed by derivation of the coordinate equations of point P and the Jacobian matrix $\mathbf{J}$ can be deduced.

$$\dot{\mathbf{X}}_{\mathrm{P}}^{1} = \mathbf{J}\dot{\boldsymbol{\theta}} \tag{3}$$

where, $\dot{\mathbf{X}}_{\mathrm{P}}^{1} = [\dot{x}_1, \dot{y}_1, \dot{z}_1]^{\mathbf{T}}$ , $\dot{x}_1 = \frac{\partial x_1}{\partial q_2}\frac{dq_2}{dt} + \frac{\partial x_1}{\partial q_3}\frac{dq_3}{dt} + \frac{\partial x_1}{\partial q_4}\frac{dq_4}{dt}$ , $\dot{z}_1 = \frac{\partial z_1}{\partial q_2}\frac{dq_2}{dt} + \frac{\partial z_1}{\partial q_3}\frac{dq_3}{dt} + \frac{\partial z_1}{\partial q_4}\frac{dq_4}{dt}$ and $\dot{\boldsymbol{\theta}} = [\dot{q}_2, \dot{q}_3, \dot{q}_4]^{\mathbf{T}}$.

The Jacobian matrix for the finger is computed as follow with $q_{234} = q_2 + q_3 + q_4$ and $q_{23} = q_2 + q_3$

$$\mathbf{J} = \begin{bmatrix} -l_4\sin q_{234} - l_3\sin q_{23} - l_2\sin q_2 & -l_4\sin q_{234} - l_3\sin q_{23} & -l_4\sin q_{234} \\ 0 & 0 & 0 \\ -l_4\cos q_{234} - l_3\cos q_{23} - l_2\cos\ q_2 & -l_4\cos q_{234} - l_3\cos q_{23} & -l_4\cos q_{234} \end{bmatrix} \tag{4}$$

## 3. Solving redundant problem

The inverse kinematics problem is of a particular interest in the case of redundant robot since it can admit infinite solutions.

On one hand, the inverse kinematics algorithm can be adapted to a redundant robot by adopting a task space. Formally, a functional constraint task is imposed to be satisfied along the end-effector task; typical constraints can include obstacle avoidance, limited joint range, singularity avoidance, … etc. This constraint is implemented analytically by adding an equation to the equation system (2) of the DGM.

On the other hand, one can find the best configuration that can optimize a certain criterion, without affecting the end effector pose. An optimization problem will be defined in this case and a procedure to solve the inverse problem based on the pseudo-inverse is adopted.

Redundant robot takes advantage from the pseudo-inverse formulation by improving its flexibility and versatility as well as allowing collisions-free motions in the workspace. A T-space component handles the control of joint angles needed to accomplish a given task and a null-space component handles the way to solve the redundancy regarding to the task.

### *3.1. Kinematic method*

An additional equation is considered based on a constraint between all joint angles. The adopted constraint defines the orientation of the last phalange given as follows.

$$\alpha = q_2 + q_3 + q_4 \tag{5}$$

The equation (5) allows to arrange the DGM as classic direct model of planar manipulator with 2 revolute joints and given by

$$\begin{cases} \overline{x}_1 = x_1 - l_4 \cos\alpha - l_1 = l_3 \cos(q_2 + q_3)\, l_3 + l_2 \cos q_2 \\ \overline{z}_1 = z_1 + l_4 \sin\alpha = -l_3 \sin(q_2 + q_3) - l_2 \sin q_2 \end{cases} \tag{6}$$

The corresponding inverse model is identified analytically to compute all possible solutions of $q_2$, $q_3$ and $q_4$, resumed in Table 3.

**Table 3.** Solutions of the IKM with an additional constraint.

| **Joint variable** | **Solution 1** | **Solution 2** |
|---|---|---|
| $\boldsymbol{q_2}$ | $q_2 = atan2(\sin q_2, \cos q_2)$ <br> $\cos q_2 = \frac{-\overline{x}_1 B - \overline{z}_1 A}{A^2+B^2}$ ; $\sin q_2 = \frac{\overline{z}_1 B - \overline{x}_1 A}{A^2+B^2}$ | |
| $\boldsymbol{q_3}$ | $q_3^1 = arcos\left(\frac{\overline{x}^2 + \overline{z}^2 - (l_3^2 + l_2^2)}{2 l_2 l_3}\right)$ | $q_3^2 = -q_3^1$ |
| $\boldsymbol{q_4}$ | $q_4 = \alpha - q_3 - q_2$ | |

with $A = -3l_3 \sin q_3$, $B = 3l_3 \cos\ q_3 + l_2$ and $\left|\frac{\overline{x}_1{}^2 + \overline{z}_1{}^2 - (l_3^2 + l_2^2)}{2 l_2 l_3}\right| \leq 1$.

*3.2. Pseudo-inverse method*

As introduced, the redundancy presents an important role in the kinematics control thus redundant joints allow a robot to cope with joint limits, singularities or collision. Further redundancy can be used to minimize joint velocities or actuator torques when end-effector follows a desired trajectory. The differential kinematics equation cannot be solved directly due to the redundancy and thus the inverse of non-square matrix $\mathbf{J}$ cannot be obtained.

A redundancy problem can be defined that for a given target joint velocity to be achieved whereas also achieving a desired end-effector velocity. Therefore, $\dot{\mathbf{X}}_1^P$ is the objective to reach, while $\dot{\boldsymbol{\theta}}$ is the target objective which is based on the kinematics model given in equation (3).

To reach the desired objective, the following optimization problem can be formulated:

$$\text{Minimise } f(\delta\boldsymbol{\theta}) = \frac{1}{2}\delta\boldsymbol{\theta}^{\mathbf{T}}\mathbf{A}\delta\boldsymbol{\theta} \tag{7}$$

Subject to

$$g(\delta\boldsymbol{\theta}) = \mathbf{J}\delta\boldsymbol{\theta} - \delta\mathbf{X} = \mathbf{0}$$

The analytical solution exists and the redundancy can be solved by the following solution: $\delta\boldsymbol{\theta} = \mathbf{J}^{+}\delta\mathbf{X}$, with $\mathbf{J}^{+} = \mathbf{A}^{-1}\mathbf{J}^{T}(\mathbf{J}\mathbf{A}^{-1}\mathbf{J}^{T})^{-1}$. This can be proven as follows.

The associated Lagrangien can be written as $L(\delta\boldsymbol{\theta}, \boldsymbol{\lambda}) = L(f, \boldsymbol{\lambda}) = f(\delta\boldsymbol{\theta}) + \boldsymbol{\lambda}^{\mathrm{T}} g(\delta\boldsymbol{\theta})$ with the vector of Lagrange multipliers $\boldsymbol{\lambda} = [\lambda_1, \lambda_2]^{\mathrm{T}}$. The solution that minimise $f(\delta\boldsymbol{\theta})$ and verify $g(\delta\boldsymbol{\theta}) = [0,0,0]^{\mathrm{T}}$, minimize also the Lagrangien $L(\delta\boldsymbol{\theta}, \boldsymbol{\lambda})$,

One can write the optimality conditions $\frac{\partial L}{\partial \delta\boldsymbol{\theta}} = \mathbf{0}$ and $\frac{\partial L}{\partial \boldsymbol{\lambda}} = \mathbf{0}$ as

$$\frac{\partial L}{\partial \delta\boldsymbol{\theta}} = 0 \quad \Rightarrow \quad \frac{\partial\big(f(\delta\boldsymbol{\theta})\big)}{\partial \delta\boldsymbol{\theta}} + \left[\frac{\partial\big(g(\delta\boldsymbol{\theta})\big)}{\partial \delta\boldsymbol{\theta}}\right]^{\mathrm{T}} \boldsymbol{\lambda} = 0 \tag{8}$$

$$\Rightarrow \quad \mathbf{A}\delta\boldsymbol{\theta} + \mathbf{J}^{\mathrm{T}}\boldsymbol{\lambda} = 0 \tag{9}$$

$$\frac{\partial L}{\partial \lambda} = 0 \quad \Rightarrow \quad g(\delta\boldsymbol{\theta}) = 0 \tag{10}$$

$$\Rightarrow \quad \mathbf{J}\delta\boldsymbol{\theta} - \delta\mathbf{X} = 0 \tag{11}$$

One can obtain,

$$\mathbf{A}\delta\boldsymbol{\theta} + \mathbf{J}^{\mathrm{T}}\boldsymbol{\lambda} = 0 \tag{12}$$

$$\mathbf{J}\delta\boldsymbol{\theta} - \delta\mathbf{X} = 0 \tag{13}$$

If $\mathbf{A}$ is considered non-singular, multiplying equation (12) by $\mathbf{A}^{-1}$ allows to compute $\delta\boldsymbol{\theta}$ and then by $\mathbf{J}$ to compute $\delta\mathbf{X}$:

$$\delta\boldsymbol{\theta} = -\mathbf{A}^{-1}\mathbf{J}^{\mathrm{T}}\boldsymbol{\lambda} \tag{14}$$

$$\delta\mathbf{X} = -\mathbf{J}(\mathbf{A}^{-1}\mathbf{J}^{\mathrm{T}})\boldsymbol{\lambda} \tag{15}$$

If $\det(\,\mathbf{J}(\mathbf{A}^{-1}\mathbf{J}^{\mathrm{T}})\,) \neq 0$, the robot considered in non-singular configuration, we obtain:

$$\boldsymbol{\lambda} = -[\mathbf{J}(\mathbf{A}^{-1}\mathbf{J}^{\mathrm{T}})]^{-1}\delta\mathbf{X} \tag{16}$$

If we substitute $\boldsymbol{\lambda}$ expression in equation (14), we obtain the analytical solution minimising the optimisation problem:

$$\delta\boldsymbol{\theta} = \mathbf{A}^{-1}\mathbf{J}^{\mathrm{T}}[\mathbf{J}(\mathbf{A}^{-1}\mathbf{J}^{\mathrm{T}})]^{-1}\delta\mathbf{X} \tag{17}$$

$$\delta\boldsymbol{\theta} = \mathbf{J}^{+}\delta\mathbf{X} \tag{18}$$

$\mathbf{J}^{+}$ is the pseudo-inverse of the Jacobean matrix $\mathbf{J}$.

A more general analytical solution to (7) projects an arbitrary vector $\mathbb{Z}$ (in joint velocity space) onto the null-space of $\mathbf{J}$, allowing to select one of the many solutions and can be obtained by minimizing the function $f(\delta\boldsymbol{\theta}) = \frac{1}{2}(\delta\boldsymbol{\theta} - \mathbb{Z})^{\mathbf{T}}\mathbf{A}(\delta\boldsymbol{\theta} - \mathbb{Z})$.

$$\delta\boldsymbol{\theta} = \mathbf{J}^{+}\delta\mathbf{x} + \mathbf{P}\mathbb{Z} \tag{19}$$

The orthogonal projection operator into the null space can be used as $\mathbf{P} = (\mathbf{I} - \mathbf{J}^{+}\mathbf{J})$. The vector $\mathbb{Z}$ can be exploited to optimize any desired criterion, without affecting the task, as joint limits or singularity avoidance for example.

## 4. Numerical implementation and validation

This section is dedicated to the numerical implementation of the proposed methods to solve the kinematics redundancy on the finger and perform the three tasks. Each method is used to solve the inverse model under Matlab and compute the joints angles as well the coordinates of point P using the DGM.

**Table 4.** The limit values of the joint angles.

| **Joint angle** | $q_2$ | $q_3$ | $q_4$ |
|---|---|---|---|
| **Maximum value** | 90° | 120° | 70° |
| **Minimum value** | 0° | 0 | 0 |

The simulations are carried out in Matlab. The frame assignments and their transformations are given out in Figure 2. The maximum and minimum joint values are shown in Table 4. The phalange length parameters are given in Table 5.

**Table 5.** The phalangeal lengths of the finger.

| | $L_1$ | $L_2$ | $L_3$ | $L_4$ |
|---|---|---|---|---|
| **Phalange length [mm]** | 152 | 45 | 35 | 32 |

### *4.1. Kinematic method implementation*

The geometric approach allows to solve the IKM but with a demerit of fixing the orientation of the last phalange given by angle $\alpha$ at equation (5) and computed on the Table 6. A solution is not

always guaranteed, which limit the T-space and so the workspace.

**Table 6.** Orientations of the last phalange.

| | **Task 1** | **Task 2** | **Task 3** |
|---|---|---|---|
| $\boldsymbol{\alpha = q_2 + q_3 + q_4}$ | 165° | 135° | 90° |

The obtained solution is partially feasible and limited regarding the computed trajectory of the fingertip. In case of task 1, the finger is not able to generate the totality of the requested trajectory. Figures 3, 4 and 5 present the computed coordinates of the point $P$ used to plot the trajectory of the fingertip for the three tasks. For each task, the initial as well as the final positions are indicated. Only for the first task the last position is not given which means that this latter is not reachable by the finger.

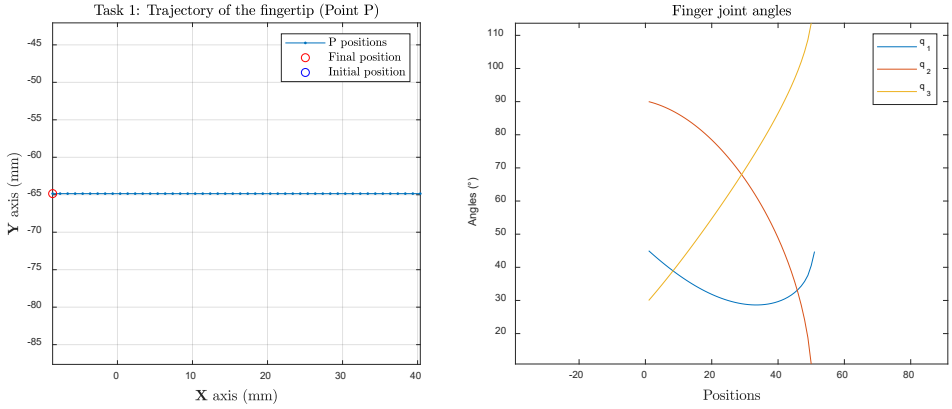


**Figure 3.** Task1 - Trajectory of the fingertip and corresponding joint angles.

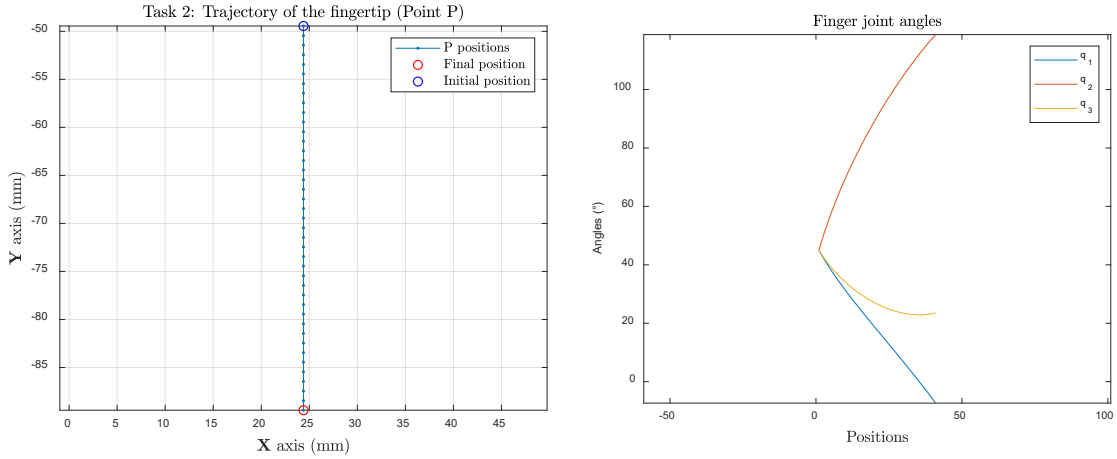


**Figure 4.** Task2 - Trajectory of the fingertip and corresponding joint angles.

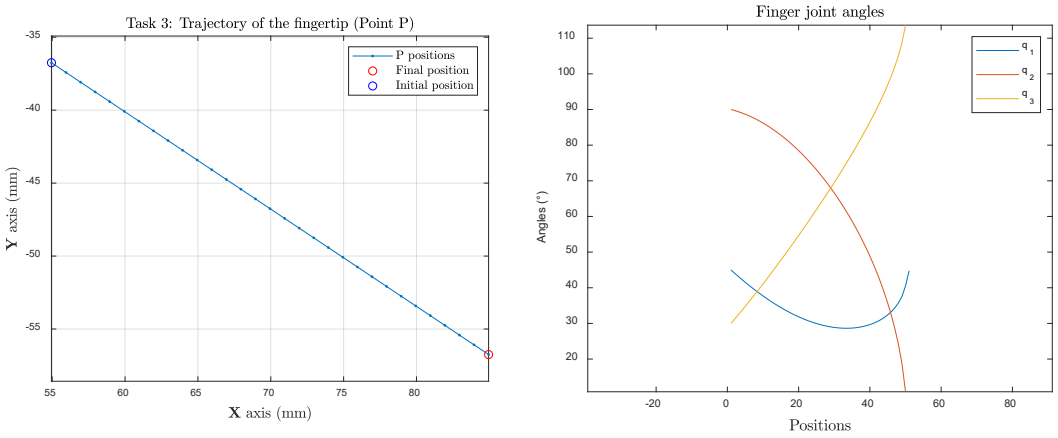


**Figure 5.** Task3 - Trajectory of the fingertip and corresponding joint angles.

### *4.2. Pseudo-inverse method implementation*

The obtained solution minimizing the optimization problem based on the pseudo-inverse of the Jacobian matrix allows to accomplish the three tasks. In order to show the feasibility of the method, all configurations of the finger are computed from the initial position to the final one and build under Matlab. In addition to this construction, the trajectory of the point $P$ as well as the finger joint angles are plotted. Figures 6, 7 and 8 present the numerical results of the implementation of the pseudo-inverse method.

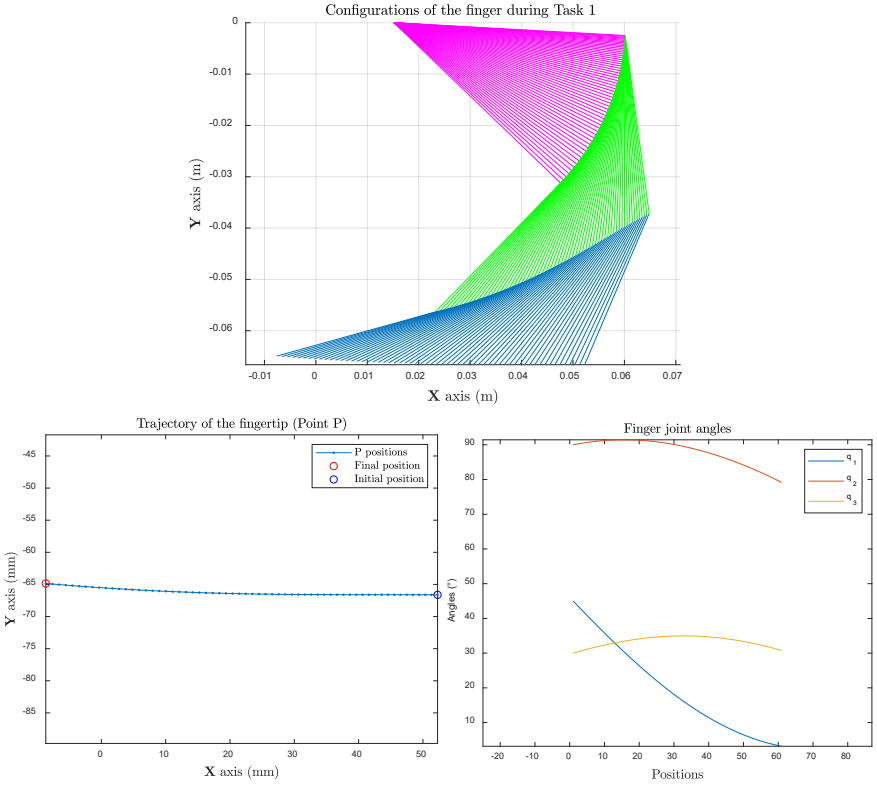


**Figure 6.** Task 1 - Numerical validation of the pseudo-inverse method: (a) Graphical finger construction (b) Trajectory of the fingertip (c) Computed joint angles of the finger.

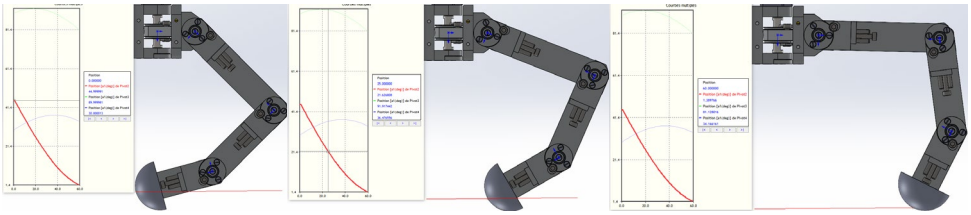

Figure 7. Task 1 - CAD simulation of the finger motion using the pseudo-inverse method.

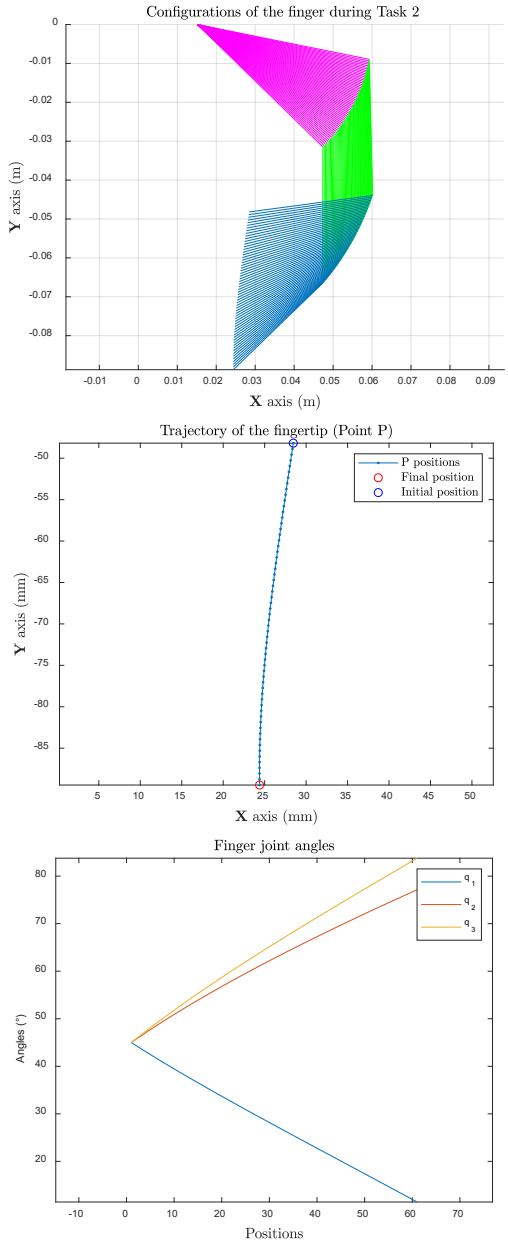


**Figure 8.** Task 2 - Numerical validation of the pseudo-inverse method: (a) Graphical finger construction (b) Trajectory of the fingertip (c) Computed joint angles of the finger.

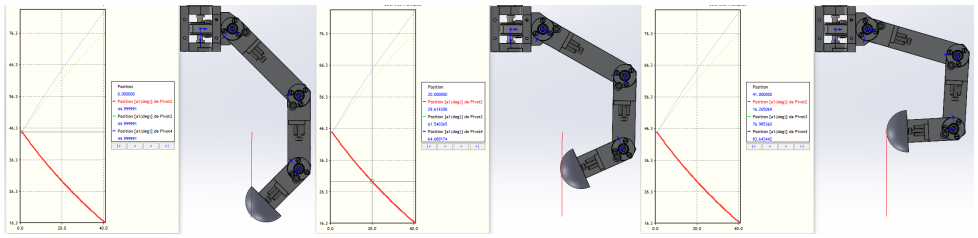

**Figure 9.** Task 2 - CAD simulation of the finger motion using the pseudo-inverse method.

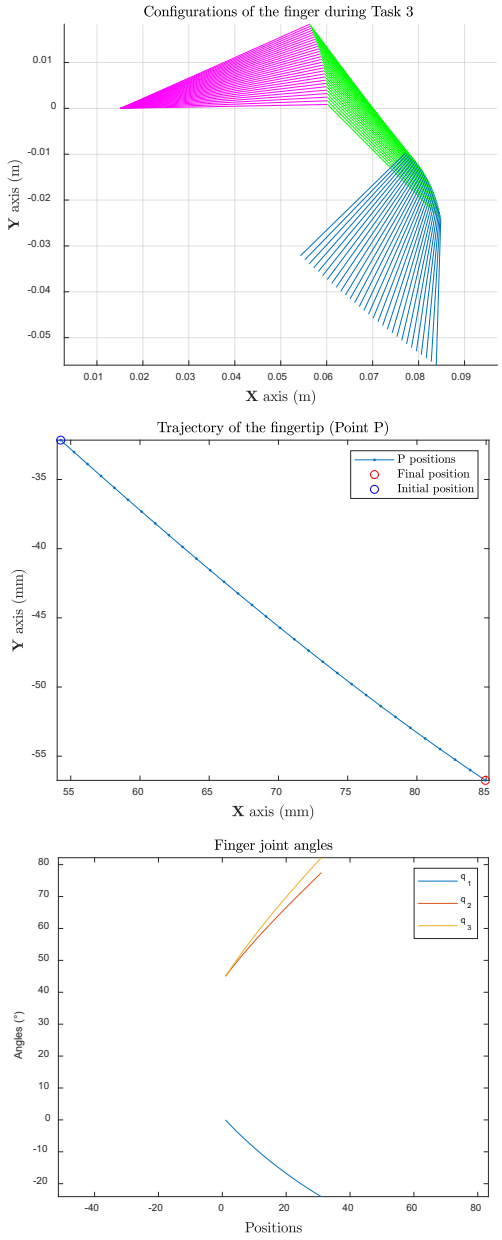


**Figure 10.** Task 3 - Numerical validation of the pseudo-inverse method: (a) Graphical finger construction (b) Trajectory of the fingertip (c) Computed joint angles of the finger.

The orientation of the last phalange for the three tasks is not fixed a shown on the graphical finger construction which is computed and updated with each configuration. Furthermore, the finger is able

to perform all tasks with no limitation in its T-space. The pseudo-inverse method is convenient and allows to identify feasible solutions unlike the geometric method.

One observes on Figures 6(c), 8(c) and 10(c) the evolution of the finger joint angles during the motion of the fingertip. All angles are inside the bounding interval defined in Table 4.

CAD simulation performed under Solidworks with the help of Meca3D software comes to validate the obtained solution. As shown on Figures 7 and 9, the finger is controlled as a serial robot with computed joint angles $q_2$, $q_3$ and $q_4$ as an input. Screen shots present the finger simulation in three positions (initial, intermediate and final) and the trajectory of the fingertip.

In the next simulations, the orthogonal projection operator into the null space is used and an adequate vector $\mathbb{Z}$ is proposed.

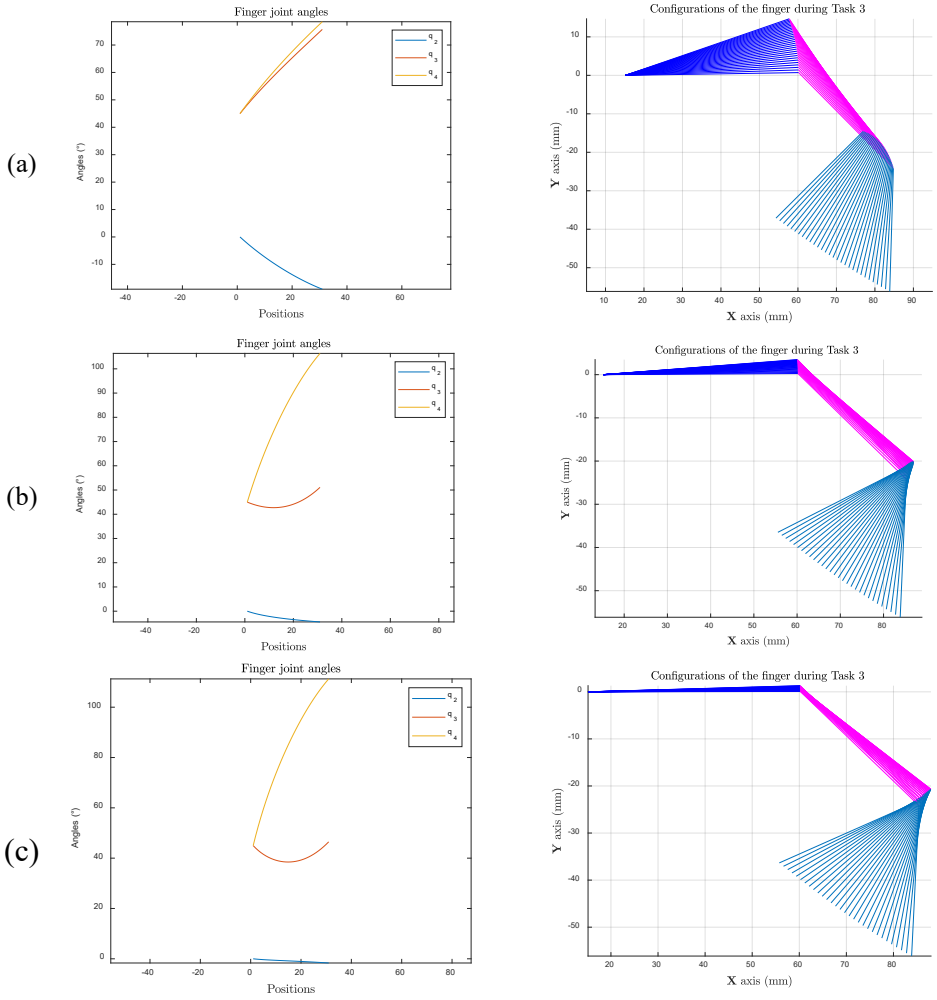


**Figure 11.** Numerical validation of the pseudo-inverse method with a criterion on the joint limits: (a) $a = 1$, $b = 1$ and $c = 1$ (b) $a = 30$, $b = 1$ and $c = 1$ (c) $a = 100$, $b = 1$ and $c = 1$.

The joint limits criterion is handled by the vector $\mathbb{Z}$ formulated as below

$$\mathbb{Z} = \varepsilon \mathbf{B}(\boldsymbol{q} - \boldsymbol{q}_m), \qquad \varepsilon < 0 \tag{20}$$

With $\mathbf{B} = \begin{bmatrix} a & 0 & 0 \\ 0 & b & 0 \\ 0 & 0 & c \end{bmatrix}$ is a diagonal matrix of weighting coefficients matrix and $\mathbf{q}_m = [q_{2m} \quad q_{3m} \quad q_{4m}]^{\mathrm{T}}$ includes the mean values of the angles based on the bounding intervals.

Three different values of the coefficient $a$ are considered to show how this choice can affects the $q_2$ joint but without changing the task. The values for $b$ and $c$ are considered equal to 1. For each value of $a$, the finger joint angles are computed and plotted on the Figure 11 (a), (b) and (c) for the values 1, 30 and 100, respectively.

The angle $q_1$ is in the vicinity to its mean value when the weighting is bigger. The criterion on joint limits is respected leading thus to suitable configurations of the finger over the three simulations. One observes the compensation of the motion by changing the two other joints, $q_3$ and $q_4$, and exploring different solutions in the null space.

## 5. Conclusion

The concept of redundancy in robotics is introduced in this paper through the study of a human finger. The biomechanical point of view allowed to establish a mechanical model of the human hand and introduce easily a finger model considered as a redundant serial robot. This latter is used to explain the definition and the theoretical description related to redundancy. The human finger model has been used to facilitate the theoretical development and to solve the inverse kinematics model. Three cases of redundancy have been considered each one linked to a specific task to execute by the fingertip. Geometric method and pseudo-inverse method have been presented and used to solve the inverse kinematics model. The limitations of the geometric method are highlighted through the obtained results. Thus, the finger is not able to generate the total trajectory and last phalangeal orientation is fixed. While, the pseudo-inverse method gives satisfaction as given by the obtained results under Matlab implementation and CAD simulation.

## References


1. Nof, S.Y. (ed.) (1985) *Handbook of Industrial Robotics*. John Wiley & Sons, New York.
2. Angeles, J. (2002) *Fundamentals of Robotic Mechanical Systems* (2nd ed.). Springer Verlag, New York.
3. Chiaverini S., Oriolo G., Maciejewski A.A. (2016) *Redundant Robots*. In: Siciliano B., Khatib O. (eds) Springer Handbook of Robotics. Springer Handbooks. Springer.
4. Conkur, E.S., Buckingham, R. (1997) Clarifying the definition of redundancy as used in robotics. *Robotica* 15(5): 583–586. DOI 10.1017/S0263574797000672.
5. Nelson, C.A., Laribi, M.A., Zeghloul, S. (2019) Multi-robot system optimization based on redundant serial spherical mechanism for robotic minimally invasive surgery. *Robotica* 37(7): 1202–1213. DOI 10.1017/S0263574718000681.
6. Saafi, H., Laribi, M.A., Zeghloul, S. (2017) Optimal torque distribution for a redundant 3-RRR spherical parallel manipulator used as a haptic medical device. *Robotics and Autonomous Systems* 89: 40-50.
7. de Wit, C.C., Siciliano, B., Bastin, G. (1996) *Theory of Robot Control*. Springer-Verlag, London.

8. Angeles, J. (2006). *Fundamentals of Robotic Mechanical Systems: Theory, Methods, and Algorithms* (3rd ed.). Springer-Verlag, New York.
9. Latash, M.L., Zatsiorsky, V.M. (2009) Multi-finger prehension: Control of a redundant mechanical system. *Advances in Experimental Medicine and Biology* 629: 597-618 https://doi.org/10.1007/978-0-387-77064-2_32
10. Towell, C., Howard, M., Vijayakumar, S. (2010) *Learning nullspace policies*. The IEEE/RSJ International Conference on Intelligent Robots and Systems, Taipei, pp. 241-248, doi: 10.1109/IROS.2010.5650663.
11. Mizera C., Laribi, M.A., Degez, D., Gazeau, J.P., Vulliez, P., Zeghloul, S. (2019) Architecture choice of a robotic hand for deep-sea exploration based on the expert gestures movements analysis. *Mechanisms and Machine Science* 72: 1-19.
12. Hu, D., Ren, L., Howad, D., Zong, C. (2014) Biomechanical analysis of force distribution in human finger extensor mechanisms. BioMed Research International, 2014: Article ID 743460, https://doi.org/10.1155/2014/743460.